ACS Photonics

Article

pubs.acs.org/journal/apchd5

UV Fluorescence Lifetime Modification by Aluminum Nanoapertures

Xiaojin Jiao,[†] Eric M. Peterson,[‡] Joel M. Harris,[‡] and Steve Blair*[,†]

[†]Department of Electrical and Computer Engineering, University of Utah, 50 South Central Campus Drive, Room 3280, Salt Lake City, Utah 84112, United States

[‡]Department of Chemistry, University of Utah, 315 South 1400 East, Room 2020, Salt Lake City, Utah 84112, United States

Supporting Information

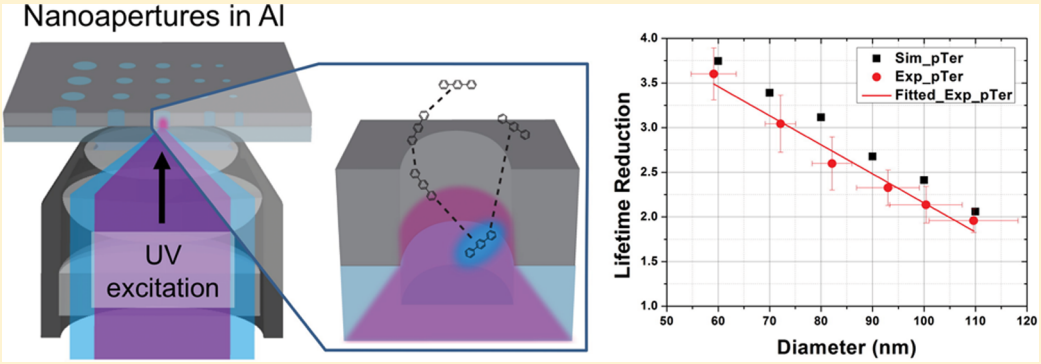

ABSTRACT: We report excited-state lifetime modification of diffusing molecules by Al nanoapertures in the UV. Lifetime reductions of ~3.5× have been observed for the high quantum yield laser dye *p*-terphenyl in a 60 nm diameter aperture. The lifetime reduction is smaller for the low quantum yield molecule tryptophan, for which a maximum reduction of ~1.7 is observed. Lifetime reduction as a function of aperture size and native quantum yield is accurately predicted by simulation. Simulation further predicts greater net fluorescence enhancement for tryptophan compared to *p*-terphenyl, which is consistent with the expectation that low quantum yield emitters experience greater enhancement in the effective quantum yield.

KEYWORDS: *plasmonics, ultraviolet, fluorescence lifetime*

There has been a recent surge of interest in UV plasmonics.[1−5] One of the motivating factors is accessing the electronic resonances of organic molecules, which lie in the UV part of the spectrum. Biomolecules such as peptides and proteins contain residues that absorb in the 220−280 nm range.[6,7] However, these aromatic residues have relatively low fluorescence quantum yields and molar extinction coefficients,[6,8] as do nucleic acids.[9] Achieving significant emission enhancement via plasmonic structures[10] could be a key enabling factor in the label-free detection of proteins[11] or DNA molecules.[12,13] Furthermore, there are numerous organic dye labels that absorb and fluoresce in the UV.[14]

To date, there have been no reports of UV plasmonic-enhanced fluorescence of freely diffusing molecules, nor has lifetime modification in the UV been reported. Arguably the most successful plasmonic nanostructure for analyzing freely diffusing molecules is the simple nanoaperture (of various shapes), which has been used extensively with visible fluorescence[15−20] as well as for the basis for novel label-free methods.[21,22] While several of these studies used Al nanoapertures, others adopted Au in order to realize greater fluorescence and local field enhancements in the visible.[23−25] However, conventional "plasmonic" metals such as Au suffer from the influence of interband transitions near the blue part of the spectrum. Therefore, studies to date of plasmonic structures in the UV have employed other metals, such as Al.[10,14,26−37] Aluminum has an interband transition near 800 nm with a Drude-like free-electron response from the visible to UV wavelengths.[38] Here, we use round Al nanoapertures to investigate UV fluorescence lifetime reduction of diffusing molecules, which is a first step toward more quantitative fluorescence analysis. We further show that the lifetime reduction depends on the native quantum yield of the molecule and is sensitive to the physical details of the nanoaperture, including undercutting of the nanoaperture into the substrate.

SIMULATION

Fluorescence Model. A fluorescent molecule can be treated as a system of three energy levels: a singlet ground state S_0, a first excited singlet state S_1, and a first excited triplet state T_1. The fluorescence count rate per molecule (CRM) in steady state is given by[39,40]

$$\mathrm{CRM} = \kappa\phi\frac{\sigma I_e}{1 + I_e/I_s} \quad (1)$$

Received: August 5, 2014
Published: November 12, 2014

where κ is the light collection efficiency (combination of the optical system and radiation profile), $\phi = k_{rad}/k_{tot}$ is the quantum yield (QY), k_{rad} and k_{nr} are the rate constants for radiative emission and nonradiative transition from S_1 to S_0, $k_{tot} = k_{rad} + k_{nr}$, the inverse of the excited state lifetime τ, σI_e is the net excitation rate, σ is the absorption cross-section, and the saturation intensity $I_s = k_{tot}/[\sigma(1 + k_{isc}/k_d)]$, where k_{isc} and k_d are the rate constants for intersystem crossing to the triplet state and relaxation to the ground state, respectively. Based on eq 1, CRM modification by plasmonic structures consists of three contributions: local increase in the excitation intensity I_e, local increase in the radiative emission k_{rad} and QY ϕ of enclosed fluorophores, and modification of the collection efficiency κ.

Energy transfer between the molecule and the structure is mediated through the radiative transition of the molecule (with the internal nonradiative rate k_{nr} unchanged). We denote k'_{rad} as the effective radiative rate of the structure and k'_{nr} as the dissipation rate of the structure, and define the parameter[40]

$$\zeta = \frac{k'_{rad} + k'_{nr}}{k_{rad}} \tag{2}$$

to represent the change in lifetime of a perfect dipole emitter (i.e., one with no internal resistive losses, with unity native QY ϕ_0). This factor can readily be obtained from simulation,[41] and does not change with the particular value of k_{rad}.

The Purcell factor represents the reduction in lifetime of the molecule,[42] and is defined as

$$f_{Purcell} = \frac{\tau}{\tau'} = \frac{k'_{rad} + k'_{nr} + k_{nr}}{k_{rad} + k_{nr}} = 1 + \phi_0(\zeta - 1) \tag{3}$$

Lifetime reduction is readily measurable, as described in Experimental Section. Note that $1/\tau$ is often referred to as the spontaneous emission rate, not to be confused with the radiative rate k_{rad}, and ϕ_0 is the native QY. The change in QY can then be expressed as

$$f_\phi = \frac{f_{rad}}{f_{Purcell}} \tag{4}$$

where $f_{rad} = k_{rad}'/k_{rad}$ is the ratio of the effective radiative rate with the influence of the plasmonic structure (k'_{rad}) and without the structure (k_{rad}).

It is clear from eq 3 that the Purcell factor for a nonideal emitter depends on its native QY ϕ_0. Stated differently, two emitters with different native quantum yields will experience different Purcell factors within the same electromagnetic environment. For an emitter with low ϕ_0, k_{nr} dominates k_{rad}, and since the structure acts through k_{rad}, ζ must be large to effect a decrease in lifetime. For the same emitter, f_ϕ is roughly proportional to f_{rad}. In contrast, for a high ϕ_0 emitter, k_{rad} dominates k_{nr}, and lifetime reduction is roughly proportional to ζ. However, since $f_{rad} \leq \zeta$, then $f_\phi \lesssim 1$. This is the origin of increased net fluorescence enhancement for molecules with low quantum yield[40,41] and also leads to the practical conclusion that it takes a "poor emitter" in the first place in order to realize enhancement via f_ϕ.

The expression for CRM can be simplified under saturated ($I_e \gg I_s$) and unsaturated ($I_e \ll I_s$) conditions

$$\text{CRM}|_{I_e \gg I_s} \rightarrow \kappa k_{rad} \Rightarrow \text{NE}|_{I_e \gg I_s} \rightarrow f_\kappa f_{rad} \tag{5}$$

$$\text{CRM}|_{I_e \ll I_s} \rightarrow \kappa\varphi\sigma I_e \Rightarrow \text{NE}|_{I_e \ll I_s} \rightarrow f_\kappa f_I \frac{f_{rad}}{f_{Purcell}} = f_\kappa f_I f_\phi \tag{6}$$

where NE represents the net fluorescence enhancement in each limit, f_I is the excitation enhancement, and f_κ is the change in collection efficiency, which we set to unity throughout the paper in order to focus on change in effective radiative rate.

Simulation Model. The nanoaperture structures considered in this paper are depicted in Figure 1 in cross section. The

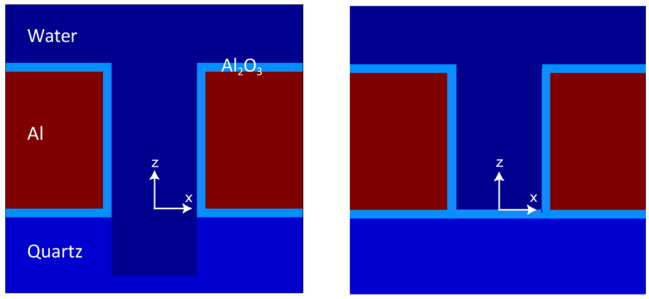

Figure 1. Cross-section views of the nanoaperture structure with (a) 50 nm undercut into the substrate and (b) an idealized case with no undercut. Oxide layer thicknesses are 4 nm.

nanoapertures are assumed to be supported by a semi-infinite glass (SiO_2) substrate and covered by water. The refractive index of water is 1.3835 at 266 nm and 1.3603 at 340 nm,[43] whereas 1-octanol, the other solvent used in our experiments, has a somewhat higher index of 1.46, measured at 325 nm;[44] all simulations used water refractive indices. Based on the fabrication method and the resulting nanoaperture structure, the model of Figure 1a has a 50 nm undercut into the substrate, while an idealized model is shown in Figure 1b with no undercut. The thicknesses of the native oxide layer along the exposed surfaces and the interfacial oxide layer at the substrate are assumed to be 4 nm. The dielectric function of Al is incorporated from measurements (see Supporting Information) and dielectric data for other materials are obtained from handbook data.

Three-dimensional electromagnetic simulation is performed using Lumerical FDTD solutions. Symmetric boundaries are used along the x and y directions according to the symmetry of the structure. Perfectly Matched Layers (PML) are used on the other boundaries. The grid size is $2 \times 2 \times 2$ nm^3. In order to calculate the excitation enhancement factor f_I, a plane wave with unit amplitude (1 V/m) is introduced inside the substrate, which normally illuminates the nanoaperture from the bottom. Average enhancement is calculated by integrating the total intensity within a volume within the aperture, and dividing by the integrated intensity within the same volume but in the absence of the Al layer. The measurement volume is a cylindrical disk of 10 nm height with diameter equal to the aperture diameter. The disk is vertically centered at a specific z-position within the aperture/undercut region.

For the emission calculations, analysis of the FDTD results use the fact that, for an atomic dipole transition that occurs through radiation, the quantum mechanical decay rate in an inhomogeneous environment can be related to the classical power radiated by the dipole in the same environment.[45]

dx.doi.org/10.1021/ph500267n | ACS Photonics 2014, 1, 1270−1277

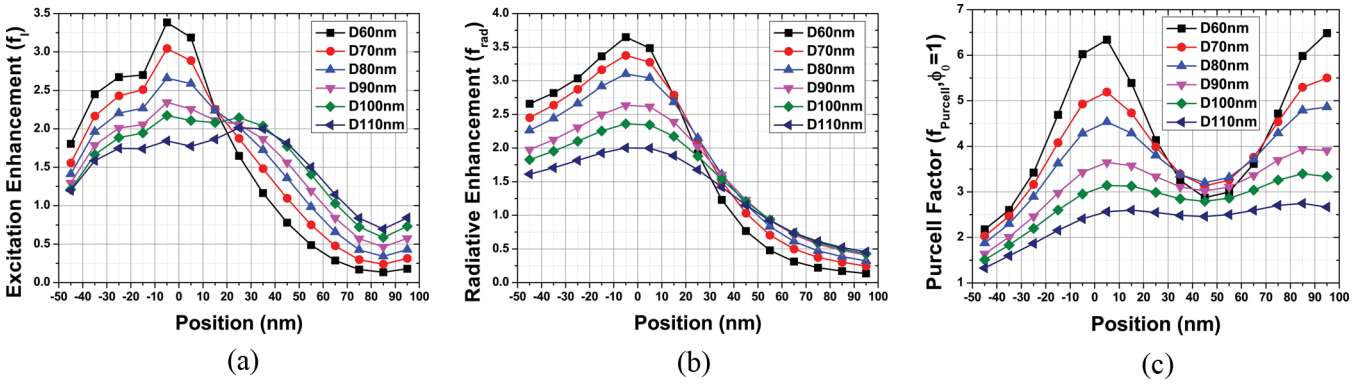

Figure 2. Calculated enhancement factors vs vertical position within the nanoaperture with a 50 nm undercut vs aperture diameter: (a) local intensity enhancement, (b) radiative enhancement into substrate, (c) Purcell factor (ϕ_0 = 1).

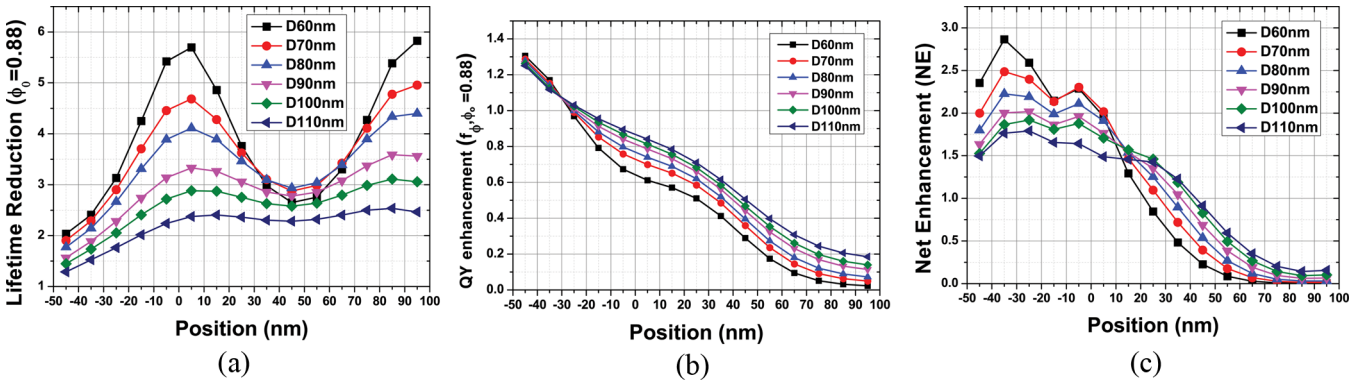

Figure 3. Calculated enhancement factors for *p*-terphenyl (ϕ_0 = 0.88) vs vertical position within a nanoaperture with a 50 nm undercut vs aperture diameter: (a) lifetime reduction, (b) change in quantum yield, and (c) net fluorescence enhancement in the regime $I_e \ll I_s$.

Specifically, every rate constant is proportional to its corresponding power, such as

$$\frac{k'_{rad}}{k'_{rad} + k'_{nr}} = \frac{P'_{rad}}{P'_0}$$

where P'_{rad} and P'_0 are the radiated and total emission power of the dipole within the plasmonic structure. An electric dipole with unit amplitude (1 V/m) is placed along the center axis of the aperture/undercut at a vertical position z. The radiated emission is calculated as the transmission through monitors around the structure, while the total emission is calculated as the transmission through monitors around the dipole. The radiative enhancement (f_{rad}) and ζ (Purcell factor, or lifetime reduction, for ϕ_0 = 1) can be calculated by dividing the corresponding emission, P'_{rad} and P'_0, respectively, by $P_0 \propto k_{rad}$, obtained in the absence of the plasmonic structure. Change in QY can then be determined from eq 4, and net enhancement can be determined from eq 5 or eq 6. Calculations are performed for the x dipole orientation only due to the symmetry of the aperture, and to the fact that the z orientation makes a negligible contribution to far-field emission,[46] which is discussed further in Supporting Information.

Simulation Results. Figure 2 shows intensity enhancement (for excitation at 270 nm), f_{rad}, and Purcell factor (ϕ_0 = 1), versus vertical position within Al nanoapertures of different diameters. A 50 nm undercut into the substrate is assumed, and the position z = 0 nm is at the interface between Al and the underlying interfacial oxide. Emission quantities are averaged over the 330 to 380 nm passband of the emission filter used in the experiments.

As expected, the maximum intensity enhancement occurs near the metal−substrate interface, with decay toward the top surface; a smaller secondary peak also exists near the metal top surface. The enhancement peaks are closer to the metal−substrate interface for the smaller aperture diameters due to the localized surface plasmon resonance (LSPR), which decreases in strength as the diameter increases. Shoulders in the enhancement curves beneath the interface are due to standing waves inside the undercut region, formed by reflections at the substrate−liquid and aperture interfaces.[47] The propagating mode cutoff condition is approached for the larger aperture diameters, giving rise to peak enhancement shifted to lie within the aperture.[48] Similarly, radiative enhancement (emission into the substrate) will decay for dipole positions toward the metal−solution interface. Due to the large Stokes shift between excitation ($\lambda \sim 270$ nm) and emission ($\lambda \sim 340$ nm), the larger apertures are well below cutoff for the emitted light, so the radiative enhancement is largely due to the LSPR. The Purcell factor reaches maximal values at both the metal−substrate interface and metal top surface due to the LSPRs at these locations. Nevertheless, lifetime reduction at the top interface would be difficult to realize with our experimental setup of bottom-side excitation/collection due to the fact that both excitation and collected emission are strongly attenuated.

Real fluorescent molecules have native quantum yields that are less than unity; Figure 3 plots lifetime reduction, change in QY, and net enhancement (in the weak excitation regime) using ϕ_0 = 0.88, which corresponds to *p*-terphenyl in our

dx.doi.org/10.1021/ph500267n | ACS Photonics 2014, 1, 1270−1277

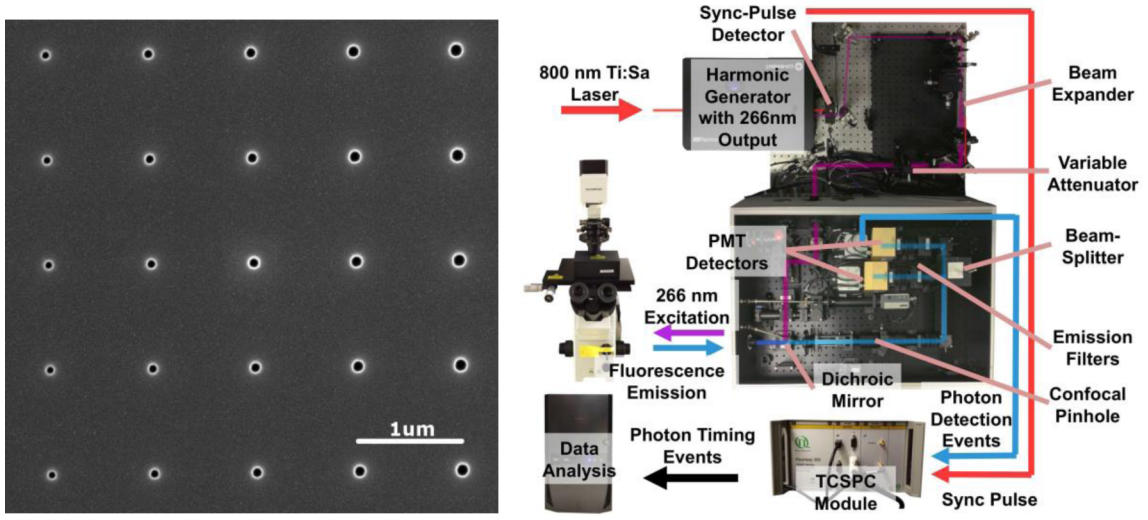

Figure 4. (a) SEM images of Al nanoaperture sample. Aperture size varies along the horizontal direction from 60 to 110 nm diameter. Milling dose varies along the vertical direction. (b) Experimental setup for lifetime measurements.

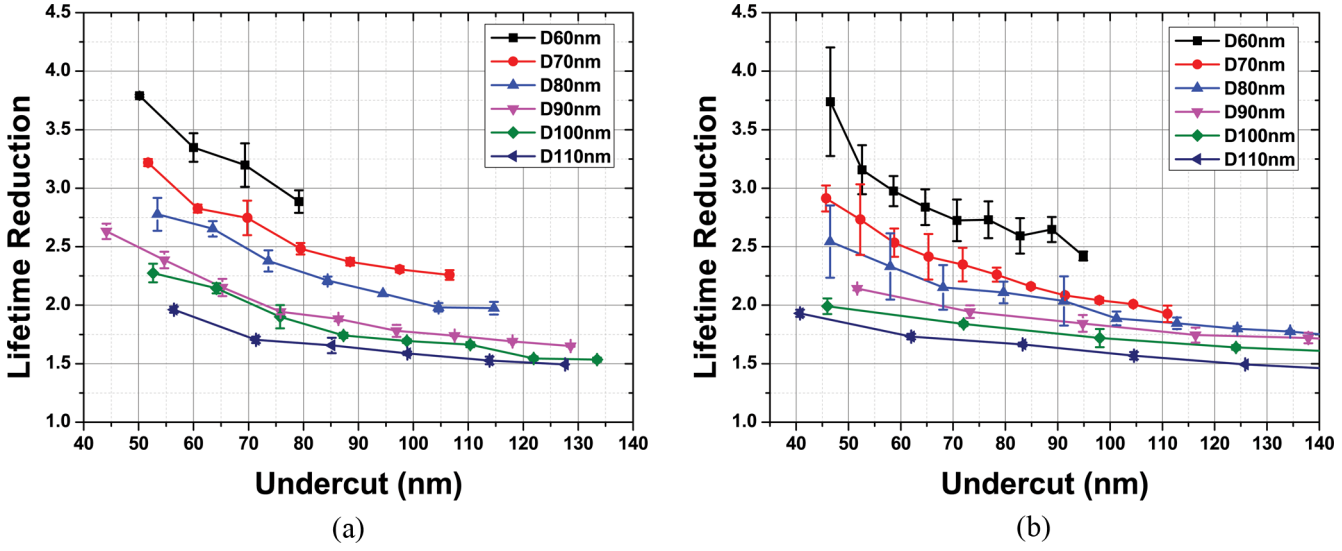

Figure 5. Measured lifetime reduction vs undercut for *p*-terphenyl with different aperture sizes. Two different nanoaperture patterns were used. Each panel represents two sets of measurements from one pattern. Error bars are standard deviations of two measurements. Uncertainty in undercut is not shown for clarity but is addressed in Figure S4. *p*-Terphenyl concentration is 100 μM in 1-octanol.

experiments. The lifetime reduction is rescaled from the situation of a perfect dipole, with maximum local value of about 5.7. Measured lifetimes will be smaller than the maximal values due to the fact that fluorescence will be detected from molecules distributed throughout the depth of the nanoaperture. This can be taken into account by performing a weighted-average of the lifetime with the net fluorescence enhancement calculated versus depth. Net enhancement is the product of f_1 and f_ϕ, and is greatest throughout the undercut region and within 10 to 20 nm above the aperture entrance due to the combination of both excitation enhancement and slight enhancement in effective QY near the interface. The maximum lifetime reduction occurs within about 20 nm of the aperture entrance; the rapid decay in lifetime reduction into the undercut region is responsible for the increase in f_ϕ beneath the aperture entrance, where $f_{rad} \gtrsim f_{Purcell}$. As a result, a 20 nm undercut would lead to an increased measured lifetime change but reduced net enhancement, as compared to a 50 nm undercut. An undercut greater than 50 nm would reduce both the measured lifetime change, and, due to rapidly decreasing f_1, the net enhancement as well.

EXPERIMENTAL SECTION

Sample Fabrication. Nanoaperture samples were fabricated on 1″-diameter quartz coverslips (200 μm thickenss). Aluminum deposition was performed by sputtering to a 100 nm thickness. Dielectric properties and composition versus depth of the Al films were obtained by spectroscopic ellipsometry and XPS analysis (see Supporting Information). Round nanoapertures were then defined by FIB milling under iodine gas injection. As shown in Figure 4a, arrays of isolated apertures were produced with aperture size varying along one direction and milling dose varying along the other direction. Two different patterns with the same design parameters were used in

dx.doi.org/10.1021/ph500267n | ACS Photonics 2014, 1, 1270−1277

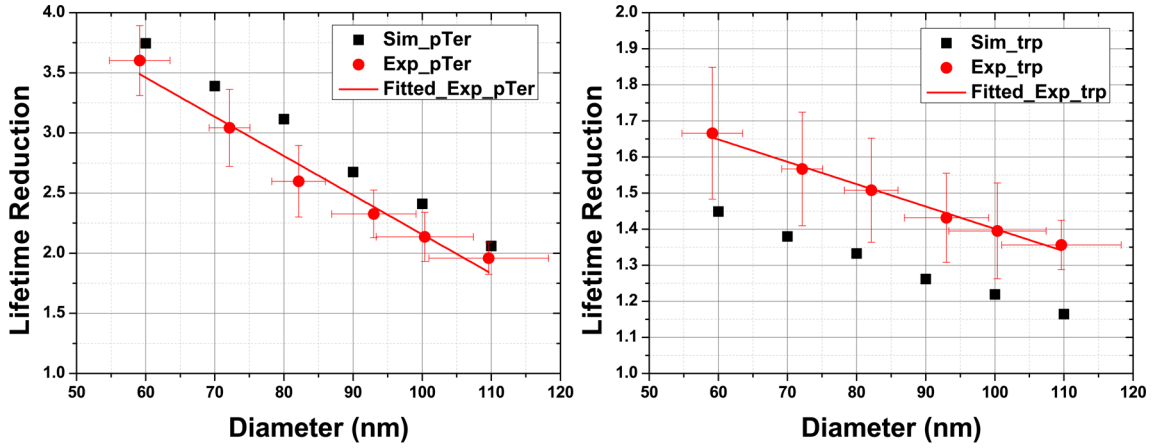

Figure 6. Measured (red) and calculated (black) lifetime reduction vs aperture diameter for (a) *p*-terphenyl (100 μM in 1-octanol) and (b) tryptophan (1 mM in 5 mM Tris pH 7.4). Experimental data points for *p*-terphenyl are based on average and standard deviation of four independent measurements (two sets on each of two patterns), while data points for tryptophan are based on the same for two independent measurements (one pattern). Uncertainty in aperture size is based on Figure S3. Linear fits are shown for the experimental data points.

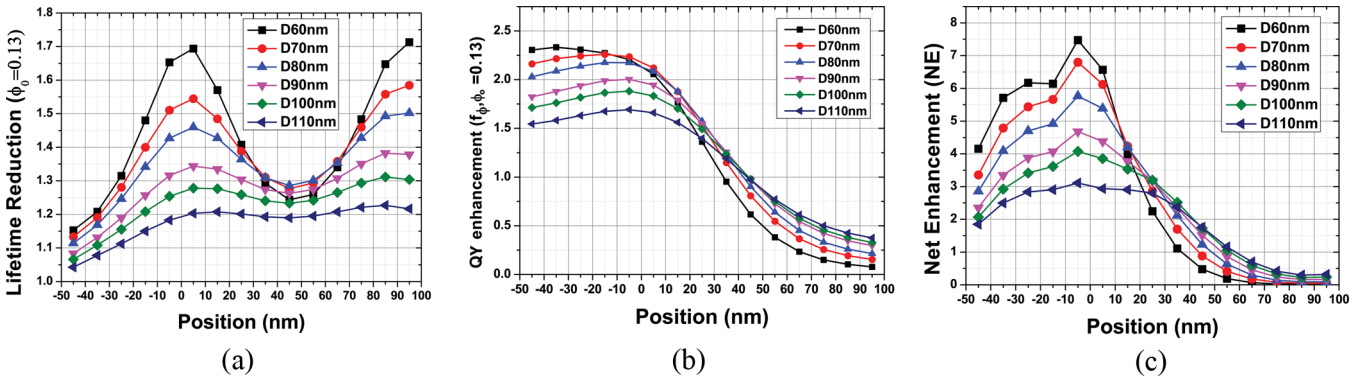

Figure 7. Calculated enhancement factors for tryptophan (ϕ_0 = 0.13) vs vertical position within a nanoaperture with a 50 nm undercut vs aperture diameter: (a) lifetime reduction, (b) change in quantum yield, and (c) net fluorescence enhancement in the regime $I_e \ll I_s$.

the experiments. Undercut versus dose for these patterns was determined by analysis of cross-section images (see Supporting Information).

Fluorescence Lifetime Measurement. The measurement setup is depicted in Figure 4b and is described in more detail in Supporting Information. The laser source is a frequency-tripled Ti:sapphire laser which provides excitation at 266 nm. Fluorescence emission is confocally imaged onto a 30 μm pinhole, and then passes through a spectral emission filter (357 ± 22 nm) before detection. The PMT output is connected to a time-correlated single-photon counting (TCSPC) unit which records photon arrival time relative to the laser pulse. Lifetimes are recovered through reconvolution of a fitted arrival-time histogram with the instrument response function (see Supporting Information).

Results. In these experiments, we investigate two fluorescing molecules with different native quantum yields. The high QY dye is *p*-terphenyl, which is a UV laser dye with measured ϕ_0 = 0.88 and τ = 0.98 ns in 1-octanol (measured at 266 nm, see Supporting Information). Measured absorption and emission peaks are near 276 and 340 nm, respectively. We also investigate tryptophan, an aromatic amino acid, which is less photochemically stable than *p*-terphenyl. Tryptophan has ϕ_0 = 0.13 in Tris buffer,[6] with measured τ = 2.95 ns, maximum absorption near 278 nm, and peak emission near 340 nm.

Figure 5 shows the measured fluorescence lifetime reduction for *p*-terphenyl versus undercut and nanoaperture diameter. Undercut calibration is discussed in Supporting Information. As expected, the lifetime reduction increases with decreasing aperture size and decreases with increasing undercut. Excitation intensities were kept below the saturation intensity, as verified by measurements of total count rate and lifetime versus input power (see Supporting Information).

In order to compare the responses of the two molecules, we extracted the lifetime reduction from ~50 nm undercut for each aperture size for both *p*-terphenyl and tryptophan. These values are plotted in Figure 6, along with calculated lifetime reduction. The calculated values were adjusted for the native quantum yields of each molecule and spatially averaged by the calculated net fluorescence enhancement. As shown, the lifetime reduction for tryptophan is significantly lower, even though both molecules experience the same photonic environment. At 100 μM concentration, we estimate that about 10 *p*-terphenyl molecules contribute to the fluorescence measured from the 60 nm aperture, and about 60 molecules contribute to fluorescence from the 110 nm aperture. At 1 mM concentration, the number of tryptophan molecules contributing to the fluorescence measurements is 10× higher.

dx.doi.org/10.1021/ph500267n | ACS Photonics 2014, 1, 1270−1277

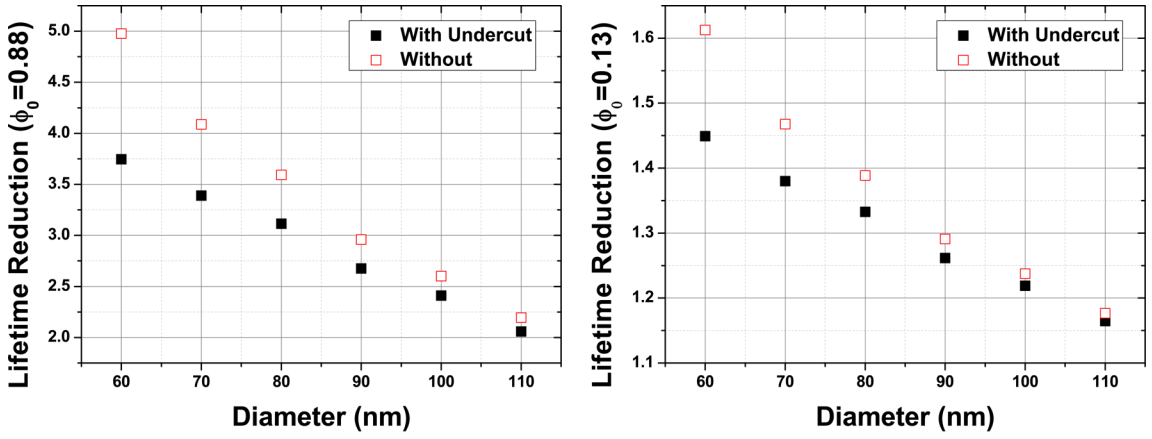

(a) (b)

Figure 8. Calculated lifetime reduction for (a) *p*-terphenyl and (b) tryptophan in nanoapertures with 50 nm undercut (ref Figure 1a) vs no undercut (ref Figure 1b).

DISCUSSION

The lifetime reduction of an emitter within a modified photonic environment is relatively straightforward to measure experimentally and estimate from simulations. As such, our experimental and simulated results (Figure 6) are in good agreement and reflect the fact that the lifetime reduction is a function of ϕ_0. To our knowledge, this relationship is not widely appreciated, but the implications are straightforward. In order to achieve an appreciable Purcell effect (e.g., $f_{\text{Purcell}} \geq 10$), the photonic structure must produce

$$\zeta \geq 1 + \frac{9}{\phi_0} \tag{7}$$

which can be difficult to achieve for poor emitters. More importantly for fluorescence detection, however, achieving a large Purcell factor is not a prerequisite for increased effective QY. Quantum yield can only be increased when $f_{\text{rad}} > f_{\text{Purcell}}$ (eq 4); f_ϕ will always be greater for a poor emitter compared to a good emitter. In contrast, in the photobleaching limit, the total number of detected photons increases by a factor f_{rad},[49,50] independent of ϕ_0. Nevertheless, for a good emitter, a large Purcell factor, even without increased QY, can lead to increased fluorescence count rate in the linear regime through an increased saturation intensity, which may be necessary for excitation enhancement to be fully utilized (but a photobleaching limit still applies). It is also clear that applications requiring large Purcell factors[51] benefit from the use of high ϕ_0 emitters.

With good agreement between experiment and calculations established for the fluorescence lifetime reduction, it is interesting to compare the predicted net fluorescence enhancement for each molecule. As shown in Figure 7 and, as expected, the local lifetime reduction is significantly smaller for tryptophan (compare to Figure 3 for *p*-terphenyl), which leads to a significant increase in QY (Figure 7b). There is an additional qualitative difference in the net enhancement in that, for tryptophan, the enhancement is predicted to be greatest near $z = 0$, due to the spatial overlap of greatest QY enhancement with excitation enhancement, compared to the maximum enhancement occurring deeper into the undercut region for *p*-terphenyl ($z \sim -35$ nm). This leads to a rather remarkable conclusion that with an undercut nanoaperture, the observation volume of the measurement is controlled by ϕ_0.

It is also interesting to further explore the effect of aperture undercut. Radiative rate enhancement, Purcell factor, and excitation enhancement for the two cases (undercut and no undercut) were calculated for varying dipole locations along the depth of the aperture (Supporting Information). Despite the difference in undercut, the results are nearly identical, with the nonundercut case being truncated at $z = 4$ nm. Experimentally, the difference between the undercut and nonundercut apertures would manifest in the lifetime reduction. Predicted lifetime reductions for the two molecules are shown in Figure 8, where the lifetime reductions are based on the lifetime versus height weighted by the net fluorescence enhancement. Because of the truncation of net fluorescence enhancement for the nonundercut case, the averaged lifetimes are weighted toward $z \sim 10$ nm where the local lifetime reductions are the greatest, whereas for the 50 nm undercut case, weighting is biased toward $z < 0$, where local lifetime reductions are rapidly decaying. Nevertheless, in terms of net fluorescence enhancement, a 50 nm undercut is advantageous.

A more efficient antenna structure could be used to increase net enhancement. From a previous numerical study of simple antenna structures in the UV,[32] which assumed the ideal case of pure Al and no surface oxidation, a dipole antenna will lead to a greater QY enhancement for low QY molecules. The bullseye aperture structure will also lead to increased effective QY due to high directionality in emission. These two structures can further lead to significant increase in local field enhancement, but a complicating factor in their design is the large Stokes shift of many molecules of interest, which requires optimization of the structures at one or both of two wavelength regions, based upon measurement requirements.

CONCLUSIONS

In summary, we have demonstrated lifetime reductions for UV chromophores in free solution using molecules with different native quantum yields. Each molecule experiences a lifetime reduction that depends on its native quantum yield, in accordance with simulation/theory. We further demonstrated that undercut of the nanoapertures into the substrate is detrimental for lifetime reduction, but simulations show that undercut can be beneficial for net fluorescence enhancement.

dx.doi.org/10.1021/ph500267n | ACS Photonics 2014, 1, 1270−1277

These results further illustrate the applicability of engineered photonic structures to different regimes of fluorescence emission modification based upon the native quantum yield of the emitter. A poor emitter can experience a large quantum yield enhancement, but with small lifetime reduction, as compared to a good emitter, which can experience a large lifetime reduction and small quantum yield enhancement (or even quantum yield reduction). A strong motivation for investigating UV plasmonics is the fact that many UV chromophores are poor emitters.

■ ASSOCIATED CONTENT

Supporting Information

Comparison of dipole emission from a nanoaperture based on dipole orientation, details of Al film and nanoaperture undercut characterization, quantum yield determination for *p*-terphenyl, details of lifetime measurements, and additional measurement and simulation results. This material is available free of charge via the Internet at http://pubs.acs.org.

■ AUTHOR INFORMATION

Corresponding Author

*E-mail: blair@ece.utah.edu.

Notes

The authors declare no competing financial interest.

■ ACKNOWLEDGMENTS

This work was supported by NSF MRSEC Grant DMR-1121252. Nanofabrication was performed at the University of Utah USTAR shared facilities, supported in part by NSF DMR-1121252. Additional support from NSF through Grant CHE-1306204 is acknowledged. We thank the reviewers for their valuable suggestions to improve the manuscript. We thank Paolo Perez for performing the XPS measurements.

■ REFERENCES

(1) Knight, M. W.; King, N. S.; Liu, L.; Everitt, H. O.; Nordlander, P.; Halas, N. J. Aluminum for plasmonics. *ACS Nano* **2014**, *8*, 834−840.
(2) Ross, M. B.; Schatz, G. C. Aluminum and indium plasmonic nanoantennas in the ultraviolet. *J. Phys. Chem. C* **2014**, *118*, 12506−12514.
(3) Rodriguez, M.; Furse, C.; Shumaker-Parry, J. S.; Blair, S. Scaling the response of nanocrescent antennas into the ultraviolet. *ACS Photonics* **2014**, *1*, 496−506.
(4) Bisio, F.; Proietti Zaccaria, R.; Moroni, R.; Maidecchi, G.; Alabastri, A.; Gonella, G.; Giglia, A.; Andolfi, L.; Nannarone, S.; Mattera, L.; Canepa, M. Pushing the high-energy limit of plasmonics. *ACS Nano* **2014**, *8*, 9239−9247.
(5) Martin, J.; Kociak, M.; Mahfoud, Z.; Proust, J.; Gérard, D.; Plain, J. High-resolution imaging and spectroscopy of multipolar plasmonic resonances in aluminum nanoantennas. *Nano Lett.* **2014**, *14*, 5517−5523.
(6) Chen, R. F. Fluorescence quantum yields of tryptophan and tyrosine. *Anal. Lett.* **1967**, *1*, 35−42.
(7) Edelhoch, H. Spectroscopic determination of tryptophan and tyrosine in proteins*. *Biochemistry* **1967**, *6*, 1948−1954.
(8) Fasman, G. D., Ed. *Practical Handbook of Biochemistry and Molecular Biology*; CRC Press: Boca Raton, FL, 1989.
(9) Crespo-Hernández, C. E.; Cohen, B.; Hare, P. M.; Kohler, B. Ultrafast excited-state dynamics in nucleic acids. *Chem. Rev.* **2004**, *104*, 1977−2020.
(10) Ray, K.; Chowdhury, M. H.; Lakowicz, J. R. Aluminum nanostructured films as substrates for enhanced fluorescence in the ultraviolet-blue spectral region. *Anal. Chem.* **2007**, *79*, 6480−6487.
(11) Szmacinski, H.; Ray, K.; Lakowicz, J. R. Metal-enhanced fluorescence of tryptophan residues in proteins: Application towards label-free bioassays. *Anal. Biochem.* **2008**, *385*, 358−364.
(12) Lakowicz, J. R.; Shen, B.; Gryczynski, Z.; D'Auria, S.; Gryczynski, I. Intrinsic fluorescence from DNA can be enhanced by metallic particles. *Biochem. Biophys. Res. Com.* **2001**, *286*, 875−879.
(13) Lakowicz, J. R.; Malicka, J.; Gryczynski, I.; Gryczynski, Z.; Geddes, C. D. Radiative decay engineering: the role of photonic mode density in biotechnology. *J. Phys. D: Appl. Phys.* **2003**, *36*, R240−R249.
(14) Aslan, K.; Previte, M. J. R.; Zhang, Y.; Geddes, C. D. Surface plasmon coupled fluorescence in the ultraviolet and visible spectral regions using Zinc thin films. *Anal. Chem.* **2008**, *80*, 7304−7312.
(15) Levene, M. J.; Korlach, J.; Turner, S. W.; Foquet, M.; Craighead, H. G.; Webb, W. W. Zero-mode waveguides for single-molecule analysis at high concentrations. *Science* **2003**, *299*, 682−686.
(16) Rigneault, H.; Capoulade, J.; Dintinger, J.; Wenger, J.; Bonod, N.; Popov, E.; Ebbesen, T. W.; Lenne, P.-F. Enhancement of single-molecule fluorescence detection in subwavelength apertures. *Phys. Rev. Lett.* **2005**, *95*, 117401.
(17) Miyake, T.; Tanii, T.; Sonobe, H.; Akahori, R.; Shimamoto, N.; Ueno, T.; Funatsu, T.; Ohdomari, I. Real-time imaging of single-molecule fluorescence with a zero-mode waveguide for the analysis of protein−protein interaction. *Anal. Chem.* **2008**, *80*, 6018−6022.
(18) Eid, J.; et al. Real-time DNA sequencing from single polymerase molecules. *Science* **2009**, *323*, 133−138.
(19) Sandén, T.; Wyss, R.; Santschi, C.; Hassane, G.; Deluz, C.; Martin, O. J. F.; Wennmalm, S.; Vogel, H. A zeptoliter volume meter for analysis of single protein molecules. *Nano Lett.* **2011**, *12*, 370−375.
(20) Punj, D.; Mivelle, M.; Moparthi, S. B.; van Zanten, T. S.; Rigneault, H.; van Hulst, N. F.; Garcia-Parajo, M. F.; Wenger, J. A plasmonic "antenna-in-box" platform for enhanced single-molecule analysis at micromolar concentrations. *Nat. Nanotechnol.* **2013**, *8*, 512−516.
(21) Pang, Y.; Gordon, R. Optical trapping of a single protein. *Nano Lett.* **2011**, *12*, 402−406.
(22) Al Balushi, A. A.; Gordon, R. Label-free free-solution single-molecule protein−small molecule interaction observed by double-nanohole plasmonic trapping. *ACS Photonics* **2014**, *1*, 389−393.
(23) Liu, Y.; Blair, S. Fluorescence enhancement from an array of sub-wavelength metal apertures. *Opt. Lett.* **2003**, *28*, 507−509.
(24) Gérard, D.; Wenger, J.; Bonod, N.; Popov, E.; Rigneault, H.; Mahdavi, F.; Blair, S.; Dintinger, J.; Ebbesen, T. W. Nanoaperture-enhanced fluorescence: Towards higher detection rates with plasmonic metals. *Phys. Rev. B* **2008**, *77*, 045413.
(25) Wenger, J.; Gérard, D.; Dintinger, J.; Mahboub, O.; Bonod, N.; Popov, E.; Ebbesen, T. W.; Rigneault, H. Emission and excitation contributions to enhanced single molecule fluorescence by gold nanometric apertures. *Opt. Express* **2008**, *16*, 3008−3020.
(26) Dörfer, T.; Schmitt, M.; Popp, J. Deep-UV surface-enhanced Raman scattering. *J. Raman Spectrosc.* **2007**, *38*, 1379−1382.
(27) Langhammer, C.; Schwind, M.; Kasemo, B.; Zorić, I. Localized surface plasmon resonances in aluminum nanodisks. *Nano Lett.* **2008**, *8*, 1461−1471.
(28) Chan, G. H.; Zhao, J.; Schatz, G. C.; Duyne, R. P. V. Localized surface plasmon resonance spectroscopy of triangular aluminum nanoparticles. *J. Phys. Chem. C* **2008**, *112*, 13958−13963.
(29) Blaber, M. G.; Arnold, M. D.; Ford, M. J. A review of the optical properties of alloys and intermetallics for plasmonics. *J. Phys.: Condens. Matter* **2010**, *22*, 143201.
(30) Mahdavi, F.; Blair, S. Nanoaperture fluorescence enhancement in the ultraviolet. *Plasmonics* **2010**, *5*, 169−174.
(31) Wu, P. C.; Kim, T.-H.; Suvorova, A.; Giangregorio, M.; Saunders, M.; Bruno, G.; Brown, A. S.; Losurdo, M. GaMg alloy nanoparticles for broadly tunable plasmonics. *Small* **2011**, *7*, 751−756.
(32) Jiao, X.; Blair, S. Optical antenna design for fluorescence enhancement in the ultraviolet. *Opt. Exp.* **2012**, *20*, 29909−29922.
(33) Li, L.; Fang Lim, S.; Puretzky, A. A.; Riehn, R.; Hallen, H. D. Near-field enhanced ultraviolet resonance Raman spectroscopy using aluminum bow-tie nano-antenna. *Appl. Phys. Lett.* **2012**, *101*, 113116.

(34) Akbay, N.; Mahdavi, F.; Lakowicz, J. R.; Ray, K. Metal-enhanced intrinsic fluorescence of nucleic acids using platinum nanostructured substrates. *Chem. Phys. Lett.* **2012**, *548*, 45−50.
(35) Schwab, P. M.; Moosmann, C.; Wissert, M. D.; Schmidt, E. W. G.; Ilin, K. S.; Siegel, M.; Lemmer, U.; Eisler, H.-J. Linear and nonlinear optical characterization of aluminum nanoantennas. *Nano Lett.* **2013**, *13*, 1535−1540.
(36) Sigle, D. O.; Perkins, E.; Baumberg, J. J.; Mahajan, S. Reproducible deep-UV SERRS on aluminum nanovoids. *J. Phys. Chem. Lett.* **2013**, *4*, 1449−1452.
(37) Maidecchi, G.; Gonella, G.; Proietti Zaccaria, R.; Moroni, R.; Anghinolfi, L.; Giglia, A.; Nannarone, S.; Mattera, L.; Dai, H.-L.; Canepa, M.; Bisio, F. Deep ultraviolet plasmon resonance in aluminum nanoparticle arrays. *ACS Nano* **2013**, *7*, 5834−5841.
(38) McMahon, J. M.; Schatz, G. C.; Gray, S. K. Plasmonics in the ultraviolet with the poor metals Al, Ga, In, Sn, Tl, Pb, and Bi. *Phys. Chem. Chem. Phys.* **2013**, *15*, 5415−5423.
(39) Blair, S.; Wenger, J. In *The Role of Plasmonic Engineering in Surface-Enhanced Fluorescence*; Geddes, C. D., Ed.; John Wiley & Sons: New York, 2008; Chapter 17.
(40) Wenger, J.; Aouani, H.; Gérard, D.; Blair, S.; Ebbesen, T. W.; Rigneault, H. Enhanced fluorescence from metal nanoapertures: physical characterizations and biophotonic applications. *Proc. SPIE* **2010**, 75770J DOI: 10.1117/12.840042.
(41) Kinkhabwala, A.; Yu, Z.; Fan, S.; Avlasevich, Y.; Müllen, K.; Moerner, W. E. Large single-molecule fluorescence enhancements produced by a bowtie nanoantenna. *Nat. Photonics* **2009**, *3*, 654−657.
(42) Purcell, E. M. Spontaneous emission probabilities at radio frequencies. *Phys. Rev.* **1946**, *69*, 681.
(43) Palik, E. D. *Handbook of Optical Constants of Solids*; Academic Press: New York, 1998.
(44) Rabouw, F. T.; den Hartog, S. A.; Senden, T.; Meijerink, A. Photonic effects on the Förster resonance energy transfer efficiency. *Nat. Commun.* **2014**, *5*, 3610.
(45) Novotny, L.; Hecht, B. *Principles of Nano-Optics*; Cambridge University Press: New York, 2006.
(46) Liu, Y.; Mahdavi, F.; Blair, S. Enhanced fluorescence transduction properties of metallic nanocavity arrays. *IEEE J. Sel. Top. Quantum Electron.* **2005**, *11*, 778−784.
(47) Tanii, T.; Akahori, R.; Higano, S.; Okubo, K.; Yamamoto, H.; Ueno, T.; Funatsu, T. Improving zero-mode waveguide structure for enhancing signal-to-noise ratio of real-time single-molecule fluorescence imaging: A computational study. *Phys. Rev. E* **2013**, *88*, 012727.
(48) Popov, E.; Nevière, M.; Wenger, J.; Lenne, P.-F.; Rigneault, H.; Chaumet, P.; Bonod, N.; Dintinger, J.; Ebbesen, T. Field enhancement in single subwavelength apertures. *J. Opt. Soc. Am. A* **2006**, *23*, 2342−2348.
(49) Hirschfeld, T. Quantum efficiency independence of the time integrated emission from a fluorescent molecule. *Appl. Opt.* **1976**, *15*, 3135−3139.
(50) Cang, H.; Liu, Y.; Wang, Y.; Yin, X.; Zhang, X. Giant suppression of photobleaching for single molecule detection via the Purcell effect. *Nano Lett.* **2013**, *13*, 5949−5953.
(51) Yablonovitch, E. Metal optics, optical antennas, and spontaneous hyper-emission. *IEEE Conf. Nanotechnol., 10th* **2010**, 13−14 DOI: 10.1109/NANO.2010.5697734 .